Astron. Astrophys. 354, 296–304 (2000)

ASTRONOMY AND ASTROPHYSICS

Acoustic waves in a stratified atmosphere

II. Three-dimensional hydrodynamics

G. Bodo[1], **W. Kalkofen**[2], **S. Massaglia**[3], **and P. Rossi**[1]

[1] Osservatorio Astronomico di Torino, Strada dell'Osservatorio 20, 10025 Pino Torinese, Italy (bodo@to.astro.it; rossi@to.astro.it)
[2] Harvard-Smithsonian Center for Astrophysics, Cambridge, MA 02138, USA (wolf@cfa.harvard.edu)
[3] Dipartimento di Fisica Generale dell'Università, Via Pietro Giuria 1, 10125 Torino, Italy (massaglia@ph.unito.it)

Received 6 October 1999 / Accepted 19 November 1999

Abstract. We investigate analytically the propagation of linear waves in a three-dimensional, nonmagnetic, isothermal atmosphere stratified in plane-parallel layers. The motivation is to study oscillations in the nonmagnetic chromosphere and to assess the limitations of one-dimensional simulations of the K_{2v} bright point phenomenon.

We consider an impulsively excited acoustic disturbance, emanating from a point source, and propagating outward as a spherical acoustic wave accompanied by an internal gravity wave. The waves amplify exponentially in the upward direction. A significant wave amplitude is therefore found only in a relatively narrow cone about the vertical. The amplitude of the wave decreases with time. Because of the lateral spread, the wave amplitude decays faster in 2D and 3D simulations than in 1D. The initial pulse, which travels at the sound speed, carries most of the energy injected into the medium. Subsequent wave crests leave the source region at ever-increasing phase speed, but slow to the sound speed as they approach the head of the wave.

Important conclusions from the 3D solution that were not anticipated from the plane-wave solution are:
1. The bulk of the energy is emitted in the upward (and downward) direction; much less goes into the horizontal direction.
2. The wave profile narrows from the initial pulse through the amplitude maxima in the wake of the pulse.
As a consequence of both points, the shock-heated regions in the wake of the initial pulse would weaken in strength and shrink in size.
3. The height at which a given wave amplitude is reached spreads outward from the symmetry axis of the disturbance as the wave propagates upward. Thus the diameter of the shock-heated region would increase as the acoustic wave travels upward in the atmosphere.

Key words: hydrodynamics – Sun: chromosphere – waves

Send offprint requests to: G. Bodo

1. Introduction

The solar chromosphere exhibits two signatures setting it apart from the underlying photosphere: an emission spectrum that characterizes its thermodynamic state, and oscillations that characterize its dynamical state. Both signatures are present in oscillations in H_{2v} and K_{2v} bright points, which arise in the emission peaks on the blue side of the central absorption features in the resonance lines of Ca II, the H and K lines in Fraunhofer's nomenclature; these features originate at a height of approximately 1 Mm above $\tau = 1$ in the nonmagnetic chromosphere.

The H and K lines are the strongest lines in the visible chromospheric spectrum and they show the three-minute oscillations. For these reasons they have often been the objects of observational studies (e.g., Liu 1974; Cram & Damè 1983; Lites, Rutten & Kalkofen 1993), and theoretical investigations (e.g., Fleck & Schmitz 1991; Kalkofen et al. 1994, hereafter KRBM; Sutmann & Umschneider 1995; Sutmann, Musielak & Ulmschneider 1998) with the aim of elucidating the excitation mechanism of the waves as well as the properties of the chromosphere.

An empirical simulation by Carlsson & Stein (1997) employing a sophisticated radiation-hydrodynamic treatment showed that the characteristic features of the spectrum of the H line emerging from the chromosphere could be predicted from the observed velocity spectrum in the photosphere on the basis of propagating acoustic waves. Their model took the photospheric velocity field observed by Lites et al. (1993) and compared the computed time-dependent emergent H line profile with the observed profile. While the model gave an emergent H line intensity during the cool phase of the wave, as well as an overall temperature structure, that are strongly contradicted by the observations (Kalkofen, Ulmschneider & Avrett 1999), the intricate velocity and intensity variations in the line core during the bright phase of the wave are reproduced to high fidelity; only in the timing of the computed H_{2v} intensity variation relative to the photospheric motion (and probably also in the absolute intensity) are there larger discrepancies from the observations. The otherwise close agreement between simulations and observations is surprising since the simulations, like all other previous theoretical studies, assume plane acoustic waves. The reality of

the wave propagation must be more complicated, however, suggesting an idealization of cylindrical symmetry. It is therefore interesting to investigate the dependence of the results on the geometry of the waves and the limitations of the assumed plane symmetry.

We model the excitation of linear hydrodynamic waves and their outward propagation in a three-dimensional, stratified, isothermal atmosphere, assuming that the interaction that gives rise to an outward traveling wave can be modeled as a pressure pulse at some reference level in the photosphere.

Unlike the 1D case, which allowed only acoustic waves to propagate, the 3D problem admits both acoustic and internal gravity waves. Our treatment of the hydrodynamic equations allows the separation of the two modes. We will focus mainly on the acoustic mode.

Questions to be examined include (1) the lateral spreading of the energy as the wave propagates upward, (2) the decay of the energy flux from its high value in the initial pulse to later oscillations in the wake of the pulse and (3) the increase of the phase velocity from the sound speed at the head of the wave to infinite phase speeds in the asymptotic limit.

The paper is structured as follows: We present the basic hydrodynamic equations in Sect. 2, describe the numerical results from the Fourier solution in Sect. 3, give the asymptotic analysis for late times in Sect. 4 and summarize the findings in Sect. 5. The appendices contain equations used in the Fourier solution of the problem.

2. The basic equations

The linearized hydrodynamic equations for adiabatic fluctuations, expressing the conservation of mass, momentum and internal energy for a gravitationally stratified, isothermal atmosphere can be written in the form:

$$\begin{aligned} \frac{\partial \rho_1}{\partial t} &= -\nabla\cdot(\rho_0 \boldsymbol{v}_1) \\ \rho_0 \frac{\partial \boldsymbol{v}_1}{\partial t} &= -\nabla p_1 - \rho_1 \boldsymbol{g} \\ \frac{\partial p_1}{\partial t} + \boldsymbol{v}_1\cdot\nabla p_0 &= a^2\left(\frac{\partial \rho_1}{\partial t} + \boldsymbol{v}_1\cdot\nabla\rho_0\right) . \end{aligned} \tag{1}$$

where p_1, ρ_1 and $\boldsymbol{v}_1$ are, respectively, the perturbed gas pressure and density and the velocity; the subscript 0 denotes the unperturbed variables; $\boldsymbol{g} = \{0, 0, g\}$ is the gravitational acceleration, $a = \sqrt{\gamma p_0/\rho_0}$ is the sound speed and γ is the ratio of specific heats. The equilibrium values of unperturbed variables have the form:

$$p_0 = p_{00}\exp(-z/H)\,,\ \rho_0 = \rho_{00}\exp(-z/H)\,,\ v_0 = 0\,,\ \text{and}$$

$$T_0 = \text{const}\,,$$

where p_{00} and ρ_{00} are, respectively, the values of pressure and density at the reference height $z = 0$; and $H = a^2/\gamma g$ is the pressure scale height.

In order to simplify the calculations it is convenient to assume the height dependence (see Lamb 1932)

$$\boldsymbol{v}_1 \propto \mathrm{e}^{z/2H}\,, \tag{2}$$

and, as a consequence,

$$p_1\,,\ \rho_1\ \propto \mathrm{e}^{-z/2H}\,. \tag{3}$$

With these assumptions and measuring space in units of twice the pressure scale height, $2H$, and time in units of $\omega_{\rm ac}^{-1} = P_{\rm ac}/2\pi$, where $P_{\rm ac} = 4\pi H/a$ is the cutoff period, Eqs. (1) become

$$\frac{\partial^4\varphi}{\partial t^4} - (\Delta - 1)\frac{\partial^2\varphi}{\partial t^2} - 4\frac{\gamma-1}{\gamma^2}\Delta_\perp\varphi = 0\,, \tag{4}$$

where φ is any of the variables (2) or (3) in non-dimensional form, i.e., $\boldsymbol{v} = \boldsymbol{v}_1/a$, $p = p_1/p_0$ and $\rho = \rho_1/\rho_0$, i.e. the 'reduced' perturbations, and Δ and $\Delta_\perp$ are Laplacian operators. Note that the reduced quantities p and ρ bear a vertical amplification as $\exp(z/2H)$ even though the actual perturbations p_1 and ρ_1 decay with z. Note also that Eq. (4) reduces to the Klein-Gordon equation in the one-dimensional limit (see, e.g., KRBM).

We perform a plane-wave analysis assuming that all variables are proportional to $\exp[i(\boldsymbol{k}\cdot\boldsymbol{r} - \omega t)]$. Eq. (4) then yields the dispersion relation

$$\omega^4 - (1 + k^2)\,\omega^2 + 4\frac{\gamma-1}{\gamma^2}k_\perp^2 = 0\,, \tag{5}$$

(Bray & Loughhead 1974), where $k^2 = k_z^2 + k_\perp^2$ is in units of $1/2H$ and ω in units of $\omega_{\rm ac}$. Eq. (5) can be solved to obtain

$$\omega^2 = \frac{1}{2}\left[\left(k^2+1\right) \pm \sqrt{\left(k^2+1\right)^2 - 16\frac{(\gamma-1)}{\gamma^2}\left(k^2 - k_z^2\right)}\right] \tag{6}$$

where the plus sign is for the two roots for *acoustic waves* and the minus sign for the two roots for *internal gravity waves*.

The solution of system (1), subject to given initial conditions at $t = 0$, can be written in the form of Fourier Integrals:

$$p = \sum_{j=1,4}\int A_j(\boldsymbol{k})\exp[i(\boldsymbol{k}\cdot\boldsymbol{r} - \omega_j t)]d\boldsymbol{k} \tag{7}$$

$$\rho = \sum_{j=1,4}\int A_j(\boldsymbol{k})F(\boldsymbol{k},\omega_j)\exp[i(\boldsymbol{k}\cdot\boldsymbol{r} - \omega_j t)]d\boldsymbol{k} \tag{8}$$

$$v_z = \sum_{j=1,4}\int A_j(\boldsymbol{k})G(\boldsymbol{k},\omega_j)\exp[i(\boldsymbol{k}\cdot\boldsymbol{r} - \omega_j t)]d\boldsymbol{k} \tag{9}$$

$$\boldsymbol{k}_\perp\cdot\boldsymbol{v}_\perp = \sum_{j=1,4}\int A_j(\boldsymbol{k})K(\boldsymbol{k},\omega_j)\exp[i(\boldsymbol{k}\cdot\boldsymbol{r} - \omega_j t)]d\boldsymbol{k} \tag{10}$$

The summation goes over four modes corresponding to the four roots of the dispersion relation (5), i.e., both acoustic and internal gravity modes travelling in two directions.

In order to obtain the values of F, G, K of Eqs. 8-10, i.e., the relation between density, velocities and pressure in the plane-wave solutions, we have Fourier analyzed system (1), derived

a set of algebraic equations (Appendix A), and determined the amplitudes $A_j(\boldsymbol{k})$ by matching the given initial conditions at $t = 0$ (Appendix B). As initial conditions we have considered a pressure pulse; the set of conditions becomes:

$$p(\boldsymbol{r}, t = 0) = \delta p \ \exp\left(-r^2/r_0^2\right)$$

$$\rho(\boldsymbol{r}, t = 0) = 0$$

$$v_z(\boldsymbol{r}, t = 0) = 0$$

$$\boldsymbol{k}_\perp \cdot \boldsymbol{v}_\perp \ (\boldsymbol{r}, t = 0) = 0$$

where δp is the amplitude of the initial perturbation and r_0 is the spatial width of the Gaussian. Note that this four conditions completely determine the solution since we have fourth order equation. The analytical form for the amplitudes $A_j(\boldsymbol{k})$ is given in Appendix B.

3. Analysis of the results and asymptotic solution

Before we solve these equations it is instructive to consider briefly the known cases of waves in one-dimensional media. For a plane wave in a stratified atmosphere the hydrodynamic equations admit only acoustic waves, but no internal gravity waves. The solution for impulsive excitation of a disturbance (see KRBM) gives an upward traveling pulse that amplifies exponentially with height; it is followed by a wake that oscillates at the acoustic cutoff period. By contrast, a plane acoustic wave due to an impulse in a homogeneous medium, for which the atmosphere of our every-day experience is a natural approximation, shows only the signal, but no wake. It is interesting to investigate the propagation of a disturbance in a 3D medium and to highlight the differences with the 1D cases. In order to gain some preliminary insight we study the asymptotic behavior of the solution in 3D.

3.1. Asymptotic analysis

Following Whitham (1974) we describe the solution in terms of a slowly varying wavetrain (i.e., with little variation in a typical wavelength and period), writing, for example, the pressure perturbation as

$$p(\boldsymbol{r}, t) \sim \mathcal{A}(\boldsymbol{r}, t) \exp(i\theta(\boldsymbol{r}, t)) \ , \tag{11}$$

where the amplitude $\mathcal{A}$ and the phase θ are slowly varying functions of position and time. We can then define a local wavenumber, $\boldsymbol{k} = \nabla\theta$, and a local frequency, $\omega = -\partial\theta/\partial t$, to obtain for the wavenumber $\boldsymbol{k}$ the equation of motion

$$\frac{\partial \boldsymbol{k}}{\partial t} + (\boldsymbol{v}_{\rm g} \cdot \nabla)\, \boldsymbol{k} = 0 \quad , \tag{12}$$

(see Eq. 11.44 in Whitham, 1974) where $\boldsymbol{v}_{\rm g}$ is the corresponding group velocity vector. The equation is valid in the limit $t \to \infty$.

According to Eq. (12), the wavenumber $\boldsymbol{k}$ is constant along group lines, which are defined by the equation, and each value of $\boldsymbol{k}$ propagates with the corresponding constant group velocity $\boldsymbol{v}_{\rm g}(\boldsymbol{k})$. From the initial pulse, given by the superposition of modes encompassing the whole spectrum of wavenumbers, each wavenumber then propagates with its own, corresponding group velocity. A particular wavenumber found at position (x, z) at time t can be obtained by solving the pair of equations

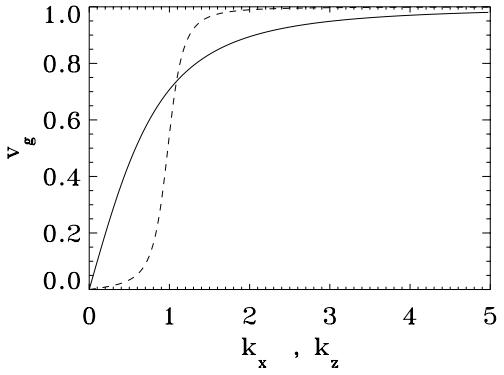

Fig. 1. Group velocity vs vertical (solid line) and horizontal (dashed line) wavenumbers.

$$x = [\boldsymbol{v}_{\rm g}(k_z, k_\perp)]_\perp t \tag{13}$$

$$z = [\boldsymbol{v}_{\rm g}(k_z, k_\perp)]_z t \, . \tag{14}$$

for the wavenumber components. The group velocity components in the vertical and horizontal directions are given by

$$(\boldsymbol{v}_{\rm g})_z = \frac{\partial\omega}{\partial k_z} = \frac{k_z}{2\omega}\left[1 + \frac{k^2+1}{\sqrt{(k^2+1)^2 - 16k_\perp^2(\gamma-1)/\gamma^2}}\right] \tag{15}$$

$$(\boldsymbol{v}_{\rm g})_\perp = \frac{\partial\omega}{\partial k_\perp} = \frac{k_\perp}{2\omega}\left[1 + \frac{k^2+1-8(\gamma-1)/\gamma^2}{\sqrt{(k^2+1)^2 - 16k_\perp^2(\gamma-1)/\gamma^2}}\right] \tag{16}$$

where ω is a root of Eq. (6) with the plus sign.

It is evident, from the dispersion relation (5) or from the system (7)–(10), that the complete solution is given by the superposition of acoustic and gravity waves. Here we confine our analysis to the acoustic waves.

The group velocity as a function of the moduli of the wavenumbers for the vertical and horizontal directions is plotted in Fig. 1, which shows that the behavior of the two curves is different at small and intermediate wavenumbers: in the horizontal direction the group velocity remains small up to $k \sim 0.7$ and then increases rapidly to the asymptotic value of unity, and in the vertical direction the growth begins steeply at $k = 0$ and then continues more gradually to the asymptotic value.

The evolution of the distribution of wavenumbers in space is described by Eqs. (13) and (14), with the group velocity $\boldsymbol{v}_{\rm g}$ given by Eqs. (15) and (16). These equations can be solved for the components k_z and $k_\perp$ in the vertical and horizontal directions as functions of z/t and x/t; the solutions are shown in Fig. 2. The two panels reflect the different behavior, described above, of the group velocity as a function of wavenumber; in both

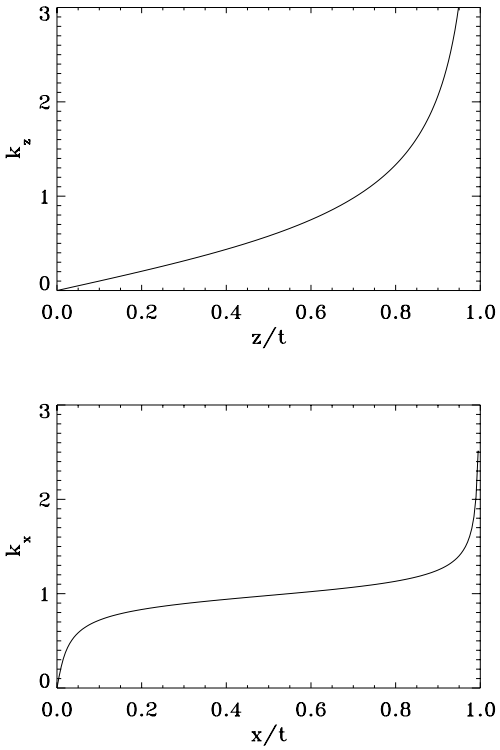

Fig. 2. Vertical (upper panel) and horizontal (lower panel) distributions of wavenumbers as a function of z/t or x/t, where t is fixed and $x, z \leq t$.

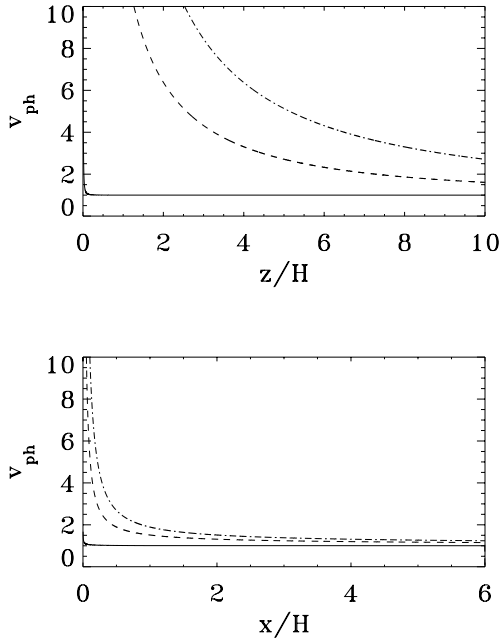

Fig. 3. Phase velocity for three consecutive maxima (solid: first maximum, dashed and dash-dotted: second and third maxima) in the vertical (upper panel) and horizontal (lower panel) directions.

cases, small wavenumbers, which have low group velocity, are found close to the origin, while large wavenumbers, which have group velocity close to the speed of sound, are found near the pulse. At intermediate distances, the distribution of k values is much broader in the vertical than in the horizontal direction. This has immediate consequences for the nature of the solution: since the value of the wavenumber found at a particular position implies also the wavelength of the oscillation, one may expect (see Fig. 6 below) that in the horizontal direction the oscillations behind the front have almost constant wavelength, while in the vertical direction the wavelength gradually increases from the head of the wave towards the origin.

Combining the phase velocity from the dispersion relation with the distribution of wavenumbers obtained from the evolution Eqs. (13) and (14) one can follow the propagation of points of constant phase, for example of a maximum. When a particular maximum is located close to the origin ($x, z = 0$) it is characterized by low values of the wavenumber, and thus high phase velocity. As it moves away from the origin, its local wavenumber as well as its frequency increase (in the vertical direction, $\omega^2 = k_z^2 + 1$), while its propagation velocity decreases (Fig. 2). Thus, as a particular maximum travels away from the origin and towards the head of the wave it is increasingly characterized by high-frequency components (which become important for shock formation in the nonlinear regime). Fig. 3 presents this behavior in more detail; it shows the phase velocity of three consecutive maxima as functions of distance from the source for the vertical (upper panel) and horizontal (lower panel) directions. In the horizontal direction the phase velocity is practically equal to the sound speed nearly throughout the whole region, and for all maxima. In the vertical direction the behavior is more complicated: Except for the head of the wave (the first maximum in Fig. 3, upper panel), which propagates at the sound speed, the later maxima have high phase velocity over increasingly extended height ranges. They therefore travel at increased phase velocity (Fig. 6, upper panel; see also KRBM Fig. 2), especially near the origin (where $v_{\rm ph} \to \infty$ as $z \to 0$), until they approach the head of the wave. As a consequence of this difference in behavior between the two directions, the surfaces of constant phase behind the wave front travel a longer distance in the vertical than in the horizontal direction and thus acquire oval shape (see Fig. 5 below).

3.2. Analysis of the results

We calculate the Fourier integral (7) numerically, taking the symmetry with respect to the z-axis into account, and interpret the results with the aid of the asymptotic analysis. Fig. 4 shows a representative solution for a pressure pulse at $x{=}z{=}t{=}0$, displaying the reduced pressure distribution, i.e., without the vertical amplification factor $\exp(z/2H)$, in a vertical plane containing the origin, at a time t corresponding to about three times the acoustic cutoff period. As discussed above, the solution is given by the superposition of acoustic and internal gravity modes. The pressure variation due to internal gravity waves, which appears as radial stripes, remains confined to the vicinity of the origin since their group velocity is lower than that of acoustic waves. It is also highly anisotropic: internal gravity waves are excluded from the purely vertical direction, and in the horizontal direction

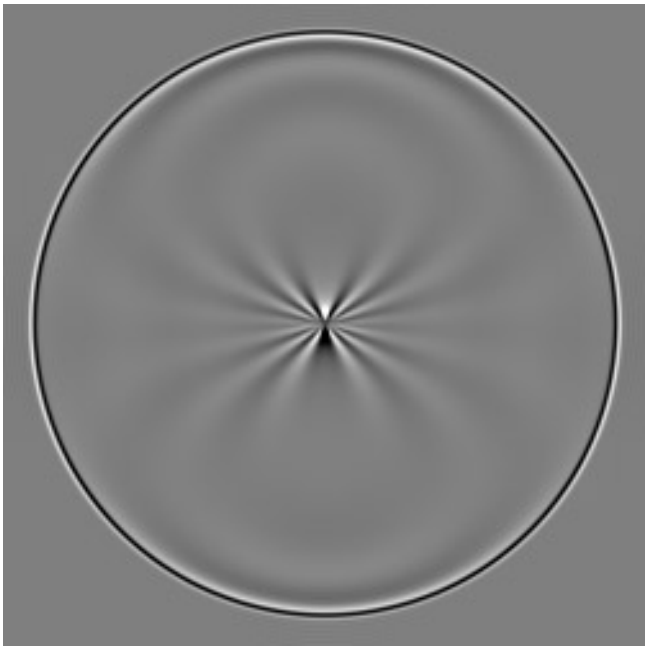

Fig. 4. Acoustic and internal gravity waves at $t = 3$ times the acoustic cutoff period, in a vertical plane through the origin. Wave crests and troughs are displayed by bright and dark shading, respectively.

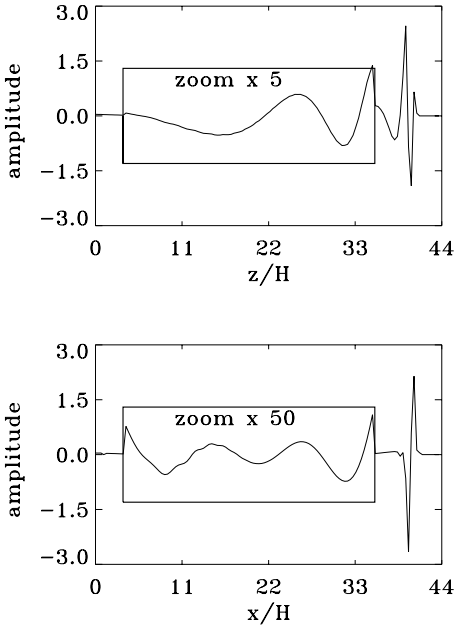

Fig. 6. Vertical (upper panel) and horizontal (lower panel) cuts of the pressure perturbation amplitude (in arbitrary units) at $t = 3$ times the acoustic cutoff period.

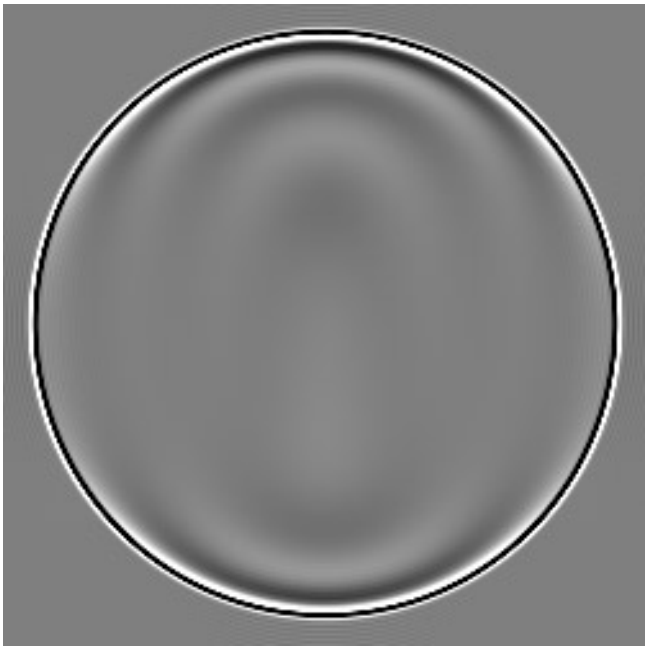

Fig. 5. Acoustic waves at $t = 3$ times the acoustic cutoff period in the vertical plane.

their group velocity reaches only about 60% of the sound speed. Because of their higher group velocity acoustic waves become more prominent at greater distance from the origin. They are seen alone in Fig. 5, which shows that the head of the wave forms a spherical surface, with radius equal to $a \times t$.

Recall that in the one-dimensional case the solution consists of a wave front followed by a wake that oscillates at a period approximately equal to the acoustic period ($\omega = 1$). In the three-dimensional case this property is found again in the vertical direction (compare Fig. 6, upper panel, and KRBM, Fig. 2), but now also in the horizontal direction, albeit with much reduced amplitude.

The oval shape of the pressure extrema is related to the distribution of $k-$values in space (Fig. 2). As seen in Fig. 6 (lower panel), the pressure amplitude in the horizontal direction has wave crests that are nearly equidistant, consistent with the narrow distribution of $k-$values and, consequently, wavelengths, through most of the range of $x-$values. By contrast, the distance between pressure extrema in the vertical direction increases with distance from the head of the wave due to the corresponding increase in the phase velocity, from the sound speed at the head of the wave to larger values near the origin (Fig. 2), (and to infinitely large values in the asymptotic limit of $t \to \infty$).

Since the disturbance is due to a point source, the wave starts out as a spherical wave. The pulse retains that shape but as can be seen in Fig. 5, the amplitude of the pulse increases from the vertical direction (both positive and negative) towards the horizontal direction.

The three-dimensional solution allows us to investigate the variation of the perturbation amplitude with direction relative to the vertical. We can look to this variation from two different perspectives: one possibility is that of considering the variation of the amplitude of a maximum at a fixed time and the other is that of considering it at a fixed height (see Fig. 7). In an astrophysical context this second case would correspond to looking at a fixed optical depth and therefore to a particular spectroscopic signature of the wave. In the first case (fixed time), the variation of the amplitude has two parts, the intrinsic variation of the

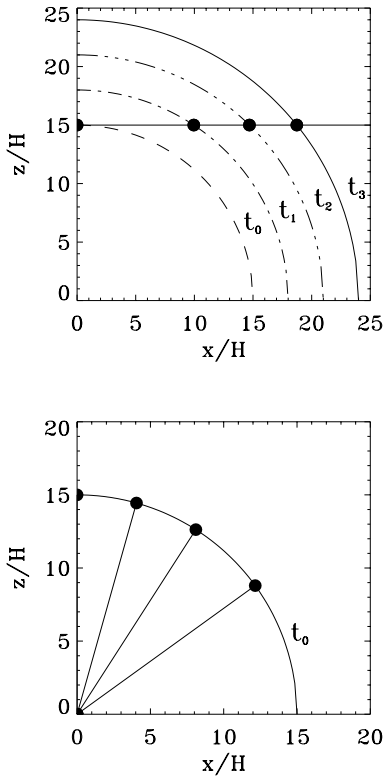

Fig. 7. Upper panel represents the positions of a wave crest at different times and their intersections with height of $15H$. Lower panel shows a wave crest whose apex has reached the height of $15H$ at time t_0.

reduced function, and the variation of the exponential factor, $\exp(z/2H)$, that compensates for the exponential dependence of the background mass density on height and converts the reduced variables into the physical variables. But at a fixed height the distinction between reduced and physical variables is irrelevant.

We consider first the case of fixed height: Fig. 8 shows the variation of the amplitude of the pulse and of the first three maxima of the wave train as they cross the height of $15H$, as functions of the angle measured relative to the vertical direction. Note that, in the actual solar chromosphere, nonlinear effects would already be present at this height for typical initial perturbations; however, our motivation is to study the basic linear behavior of the wave propagation. Since the various points of the pulse, for example, reach the target height of $15H$ with position x and hence angle increasing with time (cf.. Fig. 7), the variation of the pressure amplitude reflects partly the spherical decay of the pulse with distance r from the origin ($p \sim r^{-1}$), and partly the increase of the amplitude with angular distance from the vertical, as seen in Fig. 5. The net effect is a relatively slow decrease of the pressure amplitude, which reaches a factor of 2 at $60°$. The decay is much faster for the wave crests in the wake, reaching a factor of 10 at $60°$ for the first and second maxima, and at $40°$ for the third maximum. The wave profile evidently narrows considerably with time.

A picture complementary to Fig. 8 is shown in Fig. 9, with the angle variation of the pressure perturbation at the times when

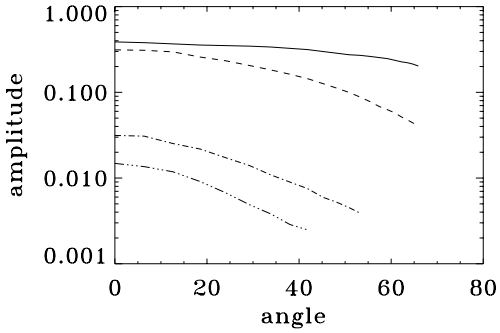

Fig. 8. Angle dependence of the (reduced) pressure amplitude relative to the vertical direction ($0°$). The values are for the fixed height of $15H$ and refer to the pulse (—), and the 1st ($--$), 2nd ($-\cdot-$) and 3rd ($-\cdots-$) maxima of the wake.

the apices of the pulse and, subsequently, of the maxima in the wake reach the height of $15H$. The upper panel gives the angle dependence of the reduced pressure (at the time when the apex reaches $z = 15H$), and the lower panel that of the physical pressure. The upper panel confirms the impression from Fig. 5 that the (reduced) pressure amplitude of the pulse grows with zenith angle. The crests of the wake weaken with separation from the vertical; they also have significantly lower amplitude. The influence of the exponential factor on the physical pressure is clearly seen in the lower panel, and it results in a much faster drop of the amplitudes with zenith angle. This is especially true for the maxima in the wake for which the oval shape causes a much faster decay than for the pulse and therefore a narrowing of the wave profile with the order of the maximum. For the pressure pulse (Fig. 9, lower panel), the decay in a half-angle of $45°$ is by nearly two orders of magnitude, and for the maxima in the wake, by nearly three orders of magnitude. Note that this decay reflects to a large extent the shape of the wave crests and is much less dramatic when the points along the crests have reached the target height, as described above.

4. The energy propagation

For the system of the linearized Eqs. (1) we can write the conservation equation for total energy in the form

$$\frac{\partial E}{\partial t} + \nabla \cdot \boldsymbol{F} = 0\,, \tag{17}$$

where the total energy density E (in units of $\rho_0 a^2$) is defined as

$$E = \frac{1}{2}\left[\boldsymbol{v}\cdot\boldsymbol{v} + \frac{p^2}{\gamma^2} + \frac{1}{2}\frac{1}{\gamma-1}\left(\frac{p}{\gamma}-\rho\right)^2\right]\,, \tag{18}$$

and the energy flux $\boldsymbol{F}$ as

$$\boldsymbol{F} = p\boldsymbol{v}. \tag{19}$$

In expression (18) for E the terms represent, respectively, kinetic energy, acoustic potential energy and gravitational potential energy. For the slowly varying wavetrain (11) we may consider

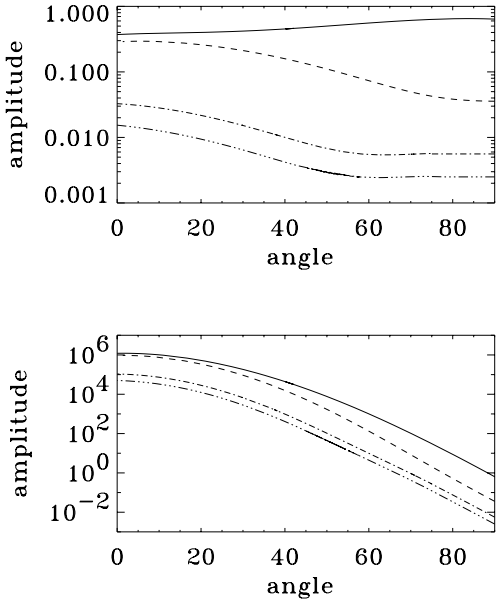

Fig. 9. Variation with zenith angle of the pulse (—), and the first three maxima of the wake (− −, − · −, − · · · −, resp.) at the instants when the apex for each feature has reached the target height of $15H$; the upper panel shows the reduced pressure, the lower panel includes the exponential height factor.

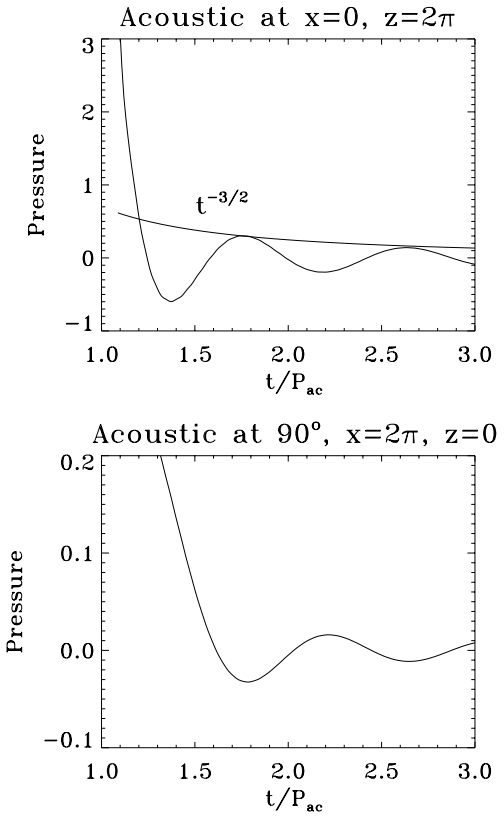

Fig. 10. Pressure amplitude of the wake (in arbitrary units) vs time at $x = 0$ and $z = 2\pi$ (top panel) and at $x = 2\pi$ and $z = 0$. The pulse has been removed; the amplitude decay of $t^{-3/2}$ is given as a comparison in the top panel.

energy and energy flux averaged over a period, denoted by $\mathcal{E}$ and $\boldsymbol{\mathcal{F}}$, where the averaged energy flux may be written as

$$\boldsymbol{\mathcal{F}} = \boldsymbol{v}_{\rm g}\mathcal{E} \tag{20}$$

(Whitham 1974, Eq. 11.69). This (asymptotically correct) form of the energy flux shows the conservation of total energy in any volume in ordinary space whose boundaries move with the group velocity according to Eqs. (13-14). Eq. (17) can therefore be written as

$$\frac{d\mathcal{E}}{dt} = -(\nabla \cdot \boldsymbol{v}_{\rm g})\,\mathcal{E}\,. \tag{21}$$

One can also read Eq. (21) noting that a positive divergence of the group lines yields a decay of the energy density. Now, since $\mathcal{E} \propto |\mathcal{A}|^2$ one can derive the temporal evolution equation for the amplitude $|\mathcal{A}|^2$,

$$\frac{d|\mathcal{A}|^2}{dt} = -n\,\frac{|\mathcal{A}|^2}{t} \tag{22}$$

(see Whitham 1974, Sect. 11.6), where n is the number of dimensions. Eq. (22) yields

$$|\mathcal{A}| \propto t^{-n/2}\,. \tag{23}$$

Fig. 10 shows the temporal decay of the reduced pressure amplitude of the wake after the pulse has reached the positions of $z = 2\pi$ on the vertical axis (top panel) and $y = 2\pi$ on the horizontal axis (lower panel). The top panel compares the decay law of $t^{-3/2}$ with the actual behavior of the wake. The agreement is excellent even though the analytic result (23) is valid only for a slowly varying wavetrain. Note the (real) time delay of $\sim P_{\rm ac}/2$ in the horizontal direction with respect to the vertical, a consequence of the phase velocity of the wake that is smaller in the horizontal direction (see Fig. 3). Note also that the amplitude of the maxima in the horizontal direction is lower by a factor of 2 to 3. This follows from the properties of the energy propagation, as will be discussed below.

At $t = 0$ the energy is spatially concentrated in the initial pulse, and as time elapses, the energy is dispersed into a wavetrain and the wavenumber distribution is spread out in ordinary space; both occur with the group velocity, as described by Eqs. (12) and (21). Thus the energy in any volume in wavenumber space remains fixed as the wavenumbers spread in physical space. Consequently

$$\mathfrak{E}(\boldsymbol{k}(x,y,z,t))\;dk_x dk_y dk_z = E(x,y,z,t)\;dxdydz\;,$$

where $E(x,y,z,t)$ is the energy per unit volume in ordinary space, estimated at the point (x,y,z) and time t, and $\mathfrak{E}(\boldsymbol{k}(x,y,z,t))$ is the energy per unit volume in the corresponding wavenumber space, where $\boldsymbol{k}(x,y,z)$ is the wavenumber at position (x,y,z) and time t. Now, volumes transform as

$$dk_x dk_y dk_z = \left|\frac{\partial(x,y,z)}{\partial(k_x,k_y,k_z)}\right|\;dxdydz\;,$$

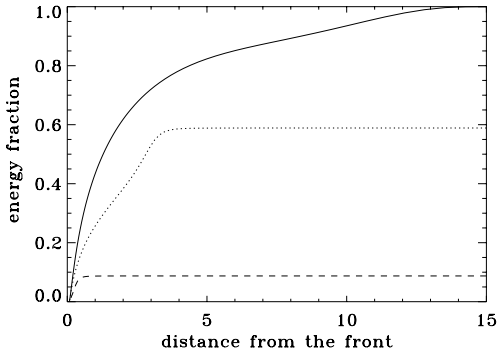

Fig. 11. The fractional energy contained inside a cone vs distance from the front, for a cone whose axis is inclined at 0° (—), 45° (· · ·), and 90° (- - -) with respect to the vertical.

where

$$\mathcal{J} = \left| \frac{\partial(x,y,z)}{\partial(k_x,k_y,k_z)} \right|$$

is the Jacobian of the tranformation between wavenumbers and ordinary space; $\mathcal{J}$ depends on the initial distribution and the expansion or contraction of volumes in the mapping from wavenumber space to ordinary space, defined by the system (13-14). The energy density can therefore be written as

$$E(x,y,z,t) = \frac{\mathfrak{E}(\boldsymbol{k}(x,y,z,t))}{\mathcal{J}} \ . \tag{24}$$

From the above discussion it is clear why the amplitude of the maxima following the pulse is much smaller in the horizontal than in the vertical direction. The behavior of the group velocity and the distribution of $k-$values in space (see Figs. 1 and 2) show that in the horizontal direction a narrow range of k values near $k = 1$ is dispersed over a large portion of physical space, while the dispersion is much lower in the vertical direction; energy is therefore much more diluted in the horizontal than in the vertical direction and, as a consequence, the maxima have much lower amplitude.

This behavior becomes even more evident from the fractional energy contained in a cone of infinitesimal opening angle when its symmetry axis points in different directions. Fig. 11 shows this fractional energy at the time when the front has reached the height of $15H$, normalized to the total energy contained in a vertical cone, against distance measured from the front of a wave. Note that in the horizontal direction the energy rises from zero at the front to the asymptotic value in $\sim 0.5H$. This implies that most of the wave energy is contained in a thin layer, of $\sim 0.5H$ width, following the pulse. But in the vertical direction about 80% of the energy is contained within a layer with a thickness of $\sim 5H$ extending in height from $10H$ to $15H$. The wake therefore contains a significant fraction of the energy. Approximately 30% of the energy is in the pulse itself, i.e., within a thin layer of $\sim 0.5H$ at the head of the wave. Note also the sharp drop of the energy with polar angle in Fig. 11. Evidently the bulk of the energy goes into the vertical direction.

5. Conclusions

We have carried out a linear analysis of the three-dimensional wave propagation in a stratified, isothermal atmosphere. The motivation was to study the limitations of the generally assumed plane waves. Although the analysis was based on linearized equations and idealized medium our results may suggest the sense in which 3D and 1D waves differ from one another in the nonlinear regime.

A pulse generated in the 'photosphere' by a 'point source' propagates upward with exponential amplification. The source region has a Gaussian pressure perturbation with a full half-width of $0.4 \times H$, where H is the pressure scale height, for a diameter of 40 km. An initial perturbation of strength $\delta p/p \approx 0.2$ becomes nonlinear at a height of $10 \times H$. So this strength of the source is near the minimum needed for $\mathrm{K_{2v}}$ bright points.

At 1 Mm above the source, which corresponds to the height of formation of the H and K lines of Ca II in the solar chromosphere, the pressure and velocity perturbations reach large values over a region with a horizontal extent of 1 Mm. This is comparable to the size of Ca bright points.

The initial pulse is followed by a wake in the upward direction at the acoustic cutoff period, approximately three minutes in the solar atmosphere. There is a wake also in the horizontal direction, with the same period but much lower amplitude.

The energy of the wave is concentrated in the vertical direction: One quarter of the upward-propagating energy is contained within a cone with a half-angle of 30° about the vertical axis; that cone constitutes only about 13% of the volume of the hemisphere. The energy is concentrated also in a narrow layer behind the initial pulse: When the wave has reached a height of $10H$ above the source, 60% of the energy on the vertical axis is contained within the first two scale heights behind the apex.

The height where a given magnitude of the perturbation is reached increases with the size of the region. Assuming that nonlinear conditions are reached on the vertical axis at a height of $10H$, a 'bright point' with a diameter of 1 Mm requires that the wave at the edge travel another $1.5H$, which requires an additional 21 s (at a sound speed of 7 km/s), and for a diameter of 2 Mm, the additinal travel distance and time are $3H$ and 45 s. Thus the 'bright point' grows from the center outward and upward. For the larger diameter and height, correspondingly higher layers in the chromosphere would form the spectrum.

The amplitude of the oscillations behind the pulse weakens in strength and shrinks in size. As a consequence, the maximal intensities associated with bright points in the wake are weaker and smaller than those in the initial pulse.

The maxima in the wake decay with time as $v(t) \propto t^{-n/2}$, depending on the geometry. For a plane wave in a one-dimensional medium, $n = 1$, the velocity decays as $t^{-1/2}$; it matches the plane wave solution of KRBM; for a line source in a two-dimensional medium, the decay is as t^{-1}; and for a point source in 3D, it is as $v(t) \propto t^{-3/2}$. The energy flux decays as $v^2(t)$. Thus the energy contained within the spherical volume of the wave decays in step with the increase in volume and hence the energy within is conserved.

For comparison with observations of chromospheric oscillations it needs to be borne in mind that the initial atmosphere in our analytic solution is at rest. The numerical simulations by Carlsson & Stein (1997) compare well with observations only when the waves are launched into a disturbed atmosphere.

Acknowledgements. This work has been supported by NASA and NSF. GB and PR thank the Smithsonian Institution for supporting their visits to CfA.

Appendix A:

System (1) can be Fourier-analyzed in terms of $\boldsymbol{v}_1, p_1, \rho_1 \propto \exp(\pm z/2H)\ \exp[i(\boldsymbol{k}\cdot\boldsymbol{r}-\omega t)]$, with the $\pm$ sign according to (2, 3), to obtain a set of algebraic equations:

$$i\omega\rho_1 + \frac{\rho_0}{2H}v_{1z} - i\boldsymbol{k}\cdot\boldsymbol{v}_1 = 0 \tag{A.1}$$

$$i\omega\rho_0\boldsymbol{v}_1 - i\boldsymbol{k}p_1 + (\frac{p_1}{2H} - g\rho_1)\hat{z} = 0 \tag{A.2}$$

$$i\omega p_1 - i\omega a^2\rho_1 - (g - \frac{a^2}{2H})\rho_0 v_{1z} = 0\,,. \tag{A.3}$$

The linearized variables can be put in a non dimensional form, as described in Sect. 2, and Eqs. (A.1), (A.2) and (A.3) can be solved to obtain $\rho = Fp\,, v_z = Gp\,, \boldsymbol{k}_\perp\cdot\boldsymbol{v}_\perp = Kp$, with F, G and K specifying relations between density, velocities and pressure in the plane-wave solutions as:

$$F(\omega,\boldsymbol{k}) = \frac{k^2 + 2ik_z - 1}{\gamma\omega^2 - 2(1-ik_z)} \tag{A.4}$$

$$G(\omega,\boldsymbol{k}) = \frac{i}{\gamma\omega}\left[\frac{\gamma\omega^2 - i\gamma\omega^2 k_z - 2(k_z^2+k^2)}{\gamma\omega^2 - 2(1-ik_z)}\right] \tag{A.5}$$

$$K(\omega,\boldsymbol{k}) = \frac{k_\perp^2}{\gamma\omega} \tag{A.6}$$

Appendix B:

The amplitudes $A_j(\boldsymbol{k})$ for an initial pressure pulse are:

$$A_1 = A_3 = \delta p\ \exp(-\frac{k^2}{k_0^2})\frac{F(\omega_2)}{F(\omega_2)-F(\omega_1)}$$

$$A_2 = A_4 = -\delta p\ \exp(-\frac{k^2}{k_0^2})\frac{F(\omega_1)}{F(\omega_2)-F(\omega_1)}\,,$$

where $k_0 = 2/r_0$, ω_1 is the solution of dispersion relation for acoustic modes and ω_2 is the solution for internal gravity modes. A_1 and A_3 are the amplitudes of acoustic modes while A_2 and A_4 are the amplitude of internal gravity modes.

References

Bray R.J., Loughhead, R.E., 1974, The Solar Atmosphere. Chapman and Hall, London
Carlsson M., Stein R.F., 1997, ApJ 481, 500
Cram L., Damé L., 1983, ApJ 272, 355
Fleck B., Schmitz F., 1991, A&A 250, 235
Kalkofen W., Rossi P., Bodo G., Massaglia S., 1994, A&A 284, 976 (KRBM)
Kalkofen W., Ulmschneider P., Avrett E.H., 1999, ApJ 521, L141
Lamb H., 1932, Hydrodynamics. Cambridge University Press, Cambridge
Lites B.W., Rutten R.J., Kalkofen W., 1993, ApJ 414, 345
Liu S.-Y., 1974, ApJ 189, 359
Sutmann G., Ulmschneider P., 1995, A&A 294, 232
Sutmann G., Musielak Z.E., Ulmschneider P., 1998, A&A 340, 556
Whitham G.B., 1974, Linear and nonlinear waves. John Wiley & Sons, New York